Received: 14 August 2024 | Revised: 18 November 2024 | Accepted: 25 February 2025 | Published online: 20 March 2025

RESEARCH ARTICLE

Medinformatics
2025, Vol. 2(3) 226–240
DOI: 10.47852/bonviewMEDIN52024089

BON VIEW PUBLISHING

Discovering Potential Therapeutic Agents for Lupus Nephritis: Insights from in Silico Research

Shahanas Naisam[1], Aswin Mohan[1], Gayathri Sreedevi Sivakumar[1], Sagarkrishna Gopalakrishnan[1] and Nidhin Sreekumar[1,*]

[1]*Department of Bioinformatics, Accubits Invent Pvt Ltd., India*

Abstract: Lupus nephritis (LN) is an enervative autoimmune disorder characterized by chronic kidney inflammation and damage. Traditional literature has highlighted the potential of various natural compounds, showcasing their diverse bioactive properties as therapeutic agents against LN. In this in silico research study, we explored the interaction analysis between 65 phytocompounds from the plants of *Ginkgo biloba*, *Boswellia serrata*, *Astragalus membranaceous*, *Withania somnifera*, *Glycyrrhiza glabra*, and *Scoparia dulcis* against 10 crucial target proteins (tumor necrosis factor, interleukin-6, matrix metalloproteinases, angiotensin-converting enzyme, nuclear factor kappa B 105, tissue inhibitor of matrix metalloproteinases, complement component 3, and complement decay-accelerating factor) associated with LN. The methodology incorporated comprehensive computational approaches, encompassing data mining, molecular property calculation, molecular docking, molecular dynamic simulation, and Molecular Mechanics/Poisson-Boltzmann Surface Area analysis. The study results indicate that 6-Prenylnaringenin is a promising candidate exhibiting stable interactions towards multiple targets, NF-kappa105 (−7.3 kcal/mol), and tumor necrosis factor (−6.6 kcal/mol). These findings suggest their potential as lead molecules for further in vitro investigation.

Keywords: lupus nephritis, autoimmune disorders, phytocompounds, molecular interaction, molecular dynamic simulation

1. Introduction

Lupus nephritis (LN), a specific consequence of systemic lupus erythematosus (SLE), is an autoimmune condition that may require harsh, protracted, and sophisticated therapy, but so far it is treatable. In an autoimmune disease, the immune system of the body attacks its cells. In LN, the immune system of the body affects the kidney's glomerular filtration unit. The delicate function of the kidneys in filtering waste from the bloodstream is impacted by the presence of LN, which leads to the accumulation of waste materials in the body [1].

The World Health Organization categorized LN for the first time in 1974. The current categorization consists of six classes: Class I, or minimal mesangial LN; Class II, or mesangial proliferative LN; Class III, or focal LN; Class IV, or diffuse LN; Class V, or membranous LN; and Class VI, or enhanced sclerosing LN [2] based on evaluating every glomerulus in a biopsy sample using light microscopy and immunofluorescence data [3, 4]. The precise origin of LN is uncertain; however, a blend of environmental and genetic aspects was the potential cause. Genes such as HLA, TLR, Fas, DNASE1, C1Q, C1R, and C1S have been associated with LN, and the formation of anti-double-stranded DNA antibodies further complicates its pathogenesis [5]. Environmental factors, including gut microbiome composition, UV radiation, pollutants, drugs, and infections, have also been linked to LN development. Certain demographics, such as younger age, male gender, and specific ethnic backgrounds, are more predisposed to LN within the context of SLE [6].

Major symptoms of LN include calcium deposition, fatigue, joint pain, high blood pressure, and edema. Calcium buildup in kidneys leads to fibrosis. Fatigue results from kidney malfunction causing waste product accumulation. Proteinuria severity varies based on LN class, presenting as foamy urine [7]. Hematuria, the presence of red blood cells in urine, is linked to renal vessel damage. Hypertension may stem from fluid retention, inflammation, vascular injury, and renin-angiotensin-aldosterone system (RAAS) activation [8]. Edema typically affects ankles, feet, legs, hands, and face. The antinuclear antibody (ANA) test is a common diagnostic tool for LN, detecting antibodies to chromatin constituents. Smith antigen-specific antibodies and those to ribosomal P, when paired with anti-dsDNA, are specific for LN [9]. Urinalysis checks for proteinuria and hematuria, and blood tests evaluate renal function using indicators like serum creatinine and ANA. Clinical examination and imaging (ultrasound, CT, MRI) assess symptoms and organ damage. Daily indicators include proteinuria, creatinine clearance, and low complement levels. Kidney biopsy defines LN class, revealing tubulointerstitial and glomerular damage. Repeated biopsies help monitor renal activity, guiding therapy in class 4 LN [10]. Non-invasive urinary biomarkers, including autoantibodies, free light chains, complement elements, and immune mediators, offer a direct and important diagnostic and predictive tool for renal diseases. Additionally, emerging therapeutic targets like tumor necrosis factor (TNF), IL-6, MMPs, ACE, NF-kappa-B, TIMPs, C3, and CD55 have been explored, offering promising avenues for more targeted and effective treatments [11].

TNF and interleukin-6 (IL-6) have emerged as potential therapeutic targets, with studies suggesting the efficacy of TNF inhibitors like infliximab and IL-6 signaling inhibitors such as

*Corresponding author: Nidhin Sreekumar, Department of Bioinformatics, Accubits Invent Pvt Ltd., India. Email: nidhin@ainvent.org

tocilizumab in reducing inflammation and improving outcomes in LN patients. Matrix metalloproteinases – MMP2 and MMP9 – play a significant role in LN, being gelatinases capable of degrading glomerular basement membrane type IV collagen. Their expression in renal biopsy specimens correlates with proliferative lesions in LN, highlighting their involvement in disease development [12]. Angiotensin-converting enzyme (ACE) is a crucial component of the RAAS and plays a key role in the pathogenesis of LN. Dysregulation of ACE contributes to renal inflammation and fibrosis, making ACE inhibitors or angiotensin II receptor blockers potential therapeutic strategies to mitigate renal damage [13]. NF-kappa-B p105 and NF-kappa-B p100 subunits, as regulators of immunity and inflammation, may contribute to LN's chronic inflammatory state. The activation of the NF-kappa-B pathway, including p100, is triggered in response to various stimuli, potentially contributing to the production of pro-inflammatory molecules in LN [14].

Tissue inhibitors of metalloproteinase 1 (TIMP1) and TIMP2, part of the tissue inhibitor of metalloproteinases family, play roles in LN by regulating matrix metalloproteinases (MMPs) involved in tissue remodeling [15]. An intricate balance between MMPs and TIMPs is crucial, as an imbalance may contribute to pathological processes in LN. Complement component 3 (C3) is a central player in the complement system, regulating blood pressure, inflammation, and immune complex clearance. Reduced serum C3 levels are associated with disease activity in SLE and LN, serving as a prognostic marker for LN treatment response [16]. CD55, also known as the decay-accelerating factor (DAF), plays a dual role in LN. While it has a protective function by inhibiting the activation of the complement system, abnormal regulation of CD55 has been implicated in autoimmune diseases, potentially contributing to inflammation and tissue damage in LN [17].

The advanced usage of herbal medicines for therapeutic purposes has tremendously increased during the past decade. The application of Ayurvedic plants is very effective in kidney diseases. *Ginkgo biloba* [18], *Boswellia serrata* [19], *Astragalus membranaceous* [20], *Withania somnifera* [21], *Glycyrrhiza glabra* [22], and *Scoparia dulcis* [23] have shown shielding properties against LN. *Ginkgo biloba* contains antioxidants and is beneficial for the circulation of blood. It has renoprotective effects from environmental pollutants like heavy metals, harmful chemicals, and toxins. *Ginkgo biloba* has been reported to be effective in treating early diabetic nephropathy [24]. The extract of *Ginkgo biloba* has been extensively used as a supplement to improve kidney function by reducing the number of Raynaud's phenomenon attacks and oxidative stress which are common in LN. *Boswellia serrata* has anti-inflammatory and analgesic properties. The active compounds in *Boswellia serrata*, such as boswellic acids, have the potential to inhibit pro-inflammatory enzymes, leading to the reduction of inflammation in the kidneys. This is particularly beneficial for kidney diseases like Lupus Nephritis (LN), where inflammation contributes to kidney damage and disease progression. Studies were reported regarding its use in the management of chronic kidney disease [25]. Active compounds of Astragalus are known to have the property of immune modulation and anti-inflammation. It helps to prevent the progression of acute kidney injury and diabetic nephropathy. The phytocompounds in Astragalus can enhance immune response while reducing inflammation which helps in normal functioning of kidney and can enhance outcomes in patients with LN. Ashwagandha has diuretic properties which help treat kidney diseases such as kidney stones [26]. It is beneficial for restoring the electrolyte balance and has curative effects on damaged microtubules which will promote the overall renal function and can make a positive impact in the treatment of LN. *Glycyrrhiza glabra* has been accredited with antioxidant and anti-apoptosis effects. *Glycyrrhiza glabra* is beneficial in the production of aldosterone and cortisone production from the adrenal cortex and is used to treat acute kidney damage [27]. The potential of *Glycyrrhiza glabra* in regulating stress response makes it a significant drug candidate in the treatment of LN. In vitro studies of *Scoparia dulcis* have shown significant dissolution action in calcium oxalate kidney stones, and it can be used to treat urolithiasis, hence called a stone melter in Malayalam. *Scoparia dulcis* can improve the renal health in individuals suffering from this autoimmune condition by reducing urolithiasis which can be a complication of LN. This study mainly aims at the bioactive compounds derived from herbal medicines, intentionally excluding standard molecules for comparison allowing us to explore more on the mechanisms of action and potential synergistic effects of these natural compounds, providing a better understanding of their therapeutic roles in LN.

This research work employs an in silico approach, integrating data mining, network analysis, molecular docking, dynamics simulations, and MMPBSA calculations to elucidate the interactions between these therapeutic targets and bioactive compounds from herbal medicines commonly used in LN treatment. *Ginkgo biloba*, *Boswellia serrata*, *Astragalus membranaceous*, *Withania somnifera*, *Glycyrrhiza glabra*, and *Scoparia dulcis* are investigated for their potential to modulate the key molecular players in LN, providing a comprehensive exploration of the intricate interplay between natural compounds and the molecular basis of LN.

2. Materials and Methods

2.1. Target identification through network analysis

The target molecules related to the disease were listed through a literature survey. The collected protein list is inputted to STRING database (https://string-db.org/) for the network and interaction data (Figure 1(A)). The protein-protein interaction network data were exported to Cytoscape software version 3.10.1 (https://cytoscape.org/) for network analysis incorporating parameters such as betweenness centrality (BC) and node degree. In this network, genes are represented as nodes, and edges denote interactions between nodes. The degree of a node indicates the number of edges connected to it; the highest degree of nodes represents significant biological function. BC assesses the importance of a node by considering the number of shortest paths passing through it. In this study, the PPI network was scrutinized using these specified parameters and the top expressed genes in the collected pool were identified (Figure 1(B)).

The ten proteins that are primarily involved in the LN pathology were selected and those proteins with limited linking to the pathway of LN or those showing functional redundancy with other proteins in the pathway were excluded. The top 10 targets include TNF, IL-6, Matrix metalloproteinase (MMP9, MMP2), Angiotensin-converting enzyme (ACE), Nuclear factor kappa B 105 (NF-kB), Tissue inhibitor matrix metalloproteinase (TIMP1 & TIMP2), Complement component 3 (C3), and Complement DAF (CD55), which were involved in the pathogenesis of LN and are considered for the study. These molecules have been implicated in the inflammatory response and immune dysregulation characteristic of LN.

The 3D structures of the targets were downloaded from the AlphaFold database [28] (Table 1). The downloaded protein structures were analyzed using Discovery Studio Visualizer software.

2.2. Ligands

A comprehensive set of phytocompounds from a range of traditional medicinal plants were chosen as ligands for the

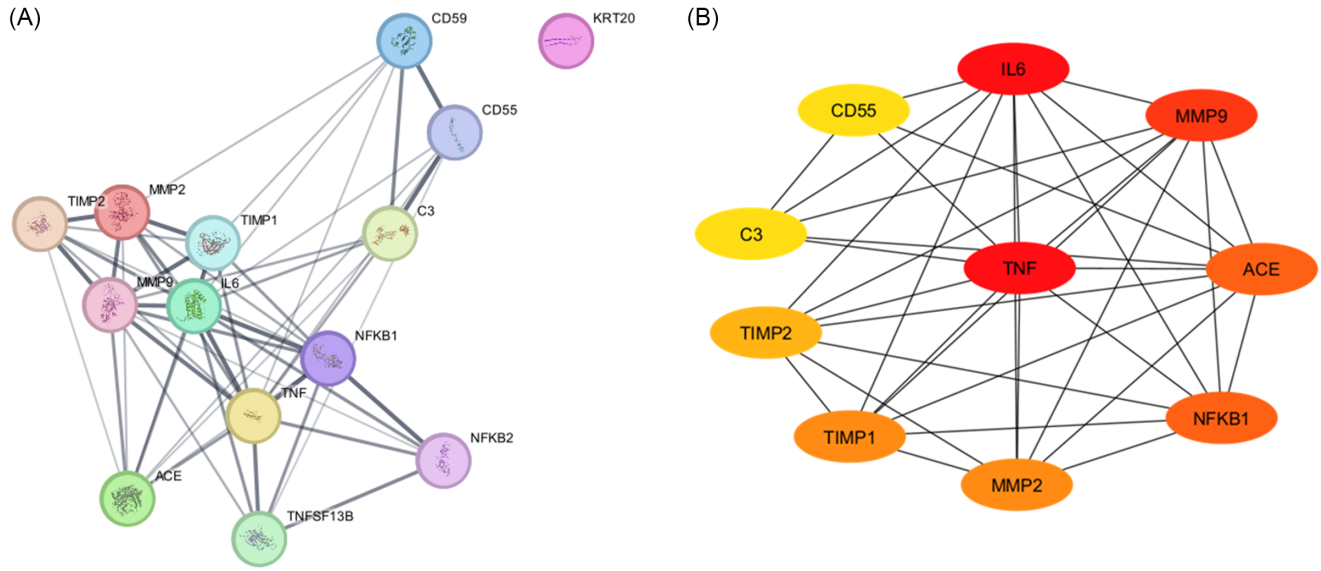

Figure 1. (A) Protein-protein networking image of the listed proteins. (B) Top 10 expressed genes

Table 1. AlphaFold structure details of targets considered for the study

Sl. No:	Protein	AlphaFold	Gene	Source organism	UniProt ID	Sequence length
1	TNF	AF-P01375-F1	TNF	Homo sapiens	P01375	231
2	IL-6	AF-P05231-F1	IL6	Homo sapiens	P05231	212
3	MMP9	AF-P14780-F1	MMP9	Homo sapiens	P14780	701
4	ACE	AF-P12821-F1	ACE	Homo sapiens	P12821	1301
5	NF-kB1	AF-P19838-F1	NFKB1	Homo sapiens	P19838	961
6	MMP2	AF-P08253-F1	MMP2	Homo sapiens	P08253	651
7	TIMP1	AF-P01033-F1	TIMP1	Homo sapiens	P01033	201
8	TIMP2	AF-P16035-F1	TIMP2	Homo sapiens	P16035	211
9	C3	AF-P01024-F1	C3	Homo sapiens	P01024	1661
10	CD55	AF-P08174-F1	CD55	Homo sapiens	P08174	381

interaction study. The selected plants included Curcumin, *Ginkgo biloba*, *Boswellia serrata*, Astragalus, Ashwagandha, *Glycyrrhiza glabra*, and *Scoparia dulcis*. These plants have a history of use in various traditional systems of medicine and are known for their anti-inflammatory and immunomodulatory properties. A total of 1526 ligands were listed. These ligands were obtained from reliable chemical databases and literature sources. The ligand structure was retrieved from small molecule database PubChem in.sdf format (https://pubchem.ncbi.nlm.nih.gov/).

2.3. Molecular and ADMET property calculation

Prior to molecular docking and interaction studies, the selected ligands underwent an initial screening based on Lipinski's Rule of Five and molecular physicochemical properties. SwissADME [29] and pkCSM [30] tools were employed to calculate the molecular properties required for screening. These industry-standard software tools enabled the calculation of molecular weight, LogP, hydrogen bond donor and acceptor counts, and other relevant physicochemical properties.

2.4. Screening of ligands

The ligands with calculated molecular properties were screened under Lipinski's Rule of Five and ADMET properties (Figure 2). Lipinski's Rule of Five or Pfizer's Rule of Five [31] is a set of guidelines used in drug discovery and medicinal chemistry to evaluate the drug-likeness and potential for oral bioavailability of chemical compounds. The Rule of Five is based on the idea that certain physicochemical properties of a compound can influence its ability to be absorbed through the gut wall and enter the bloodstream effectively. The rule criteria include the following:

1) Molecular weight: The molecular weight of the compound should be less than 500 daltons (Da). This guideline helps ensure that the compound is small enough to be efficiently absorbed in the gastrointestinal tract.
2) Lipophilicity (LogP): The calculated partition coefficient (LogP) of the compound should be less than 5. This parameter indicates the compound's hydrophilic/hydrophobic balance and influences its solubility and absorption.
3) Hydrogen bond donors: The compound should have no more than 5 hydrogen bond donor atoms (nitrogen and oxygen). Hydrogen bond donors play a role in interactions with biological receptors.
4) Hydrogen bond acceptors: The compound should have no more than 10 hydrogen bond acceptor atoms (nitrogen and oxygen). Hydrogen bond acceptors also influence interactions with biological molecules.

ADMET calculations involve assessing the absorption, distribution, metabolism, excretion, and toxicity properties of a

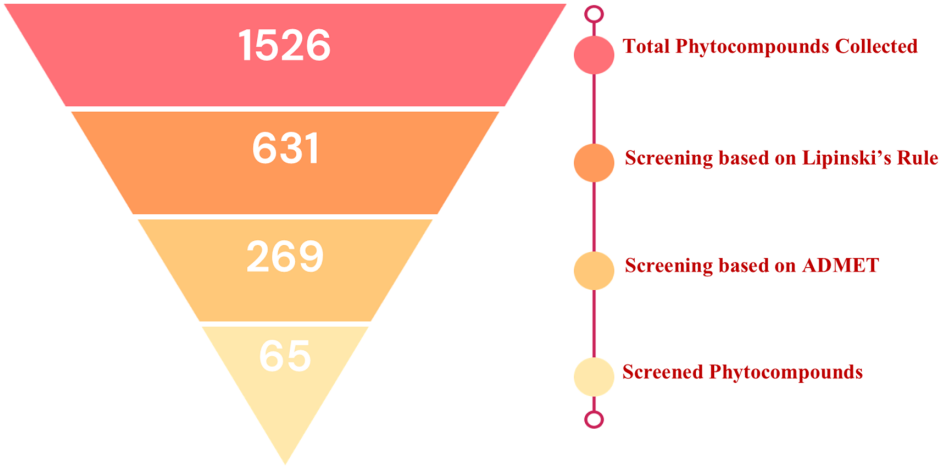

Figure 2. Screening process of phytocompounds

pharmaceutical compound. The process plays a crucial role in drug discovery and development by helping to predict the behavior of compounds within the body. Among the listed ligands, only 65 satisfied the rule and filtering parameters (Table 2).

The 2D structures of the considered phytocompounds were downloaded from PubChem [31] database in.sdf format. Subsequently, the ligands were converted into. pdbqt format using OpenBabel [32].

2.5. Molecular docking

The AutoDock Vina software (v.1.2.0.) was employed for the molecular docking analysis of the selected Proteins and ligands [33]. Primarily, the ligand structure retrieved from PubChem was prepared using Open Babel software 2.4.1. Prior docking steps such as the addition of polar hydrogen, Kollman charges, and grid box generation were carried out in the purified protein structure. The grid box was defined using the Graphical interface program of the AutoDock tool with a grid spacing of 1 Å for ten proteins and Table 3 shows the corresponding grid box value of considered proteins. The resulting prepared structure was saved in. pdbqt format. AutoDock Vina calculates and generates the top 10 protein-ligand interaction poses based on binding affinity.

2.6. Molecular interaction analysis

The molecular interaction analysis of the docked protein ligands (complex) was performed using Discovery Studio Visualizer 2017 (https://discover.3ds.com/discovery-studio-visualizer-download). The dock complex was analyzed, screened, and ranked based on binding affinity and H-bond interactions. The poses with the lowest binding affinity and the highest number of H-bonds were considered for further analysis, i.e., molecular dynamic simulation study.

2.7. Molecular dynamics simulation

Molecular dynamics simulations of the selected protein-ligand complexes were conducted using the GROMACS version 2020.6 MD package [34, 35]. The process commenced with the removal of crystal water from the protein and ligand complex, followed by the generation of topology files separately for both molecules. The protein topology file was created using the Charmm36 force field (Charmm36-jul 2021.ff). For ligands, the topology file was prepared through the CGenFf server. The box dimensions were 8.276 × 8.353 × 6.398 nm, with a volume of 442.24 nm^3 and updated configuration expands these dimensions to 10.276 ×

Table 2. Ligands considered for the in silico analysis

Sl No:	Plant	Phytocompound *(PubChem ID)*	
1	*Ginkgo biloba*	• *1,3-Dimethoxybenzene (9025)*	• *1,4-Dimethoxybenzene (9016)*
		• *2,5-Diisopropyl-P-Xylene (2521)*	• *Cianidanol (9064)*
		• *Allantoin (204)*	• *Cis-3-Hexen-1-Ol (5281167)*
		• *Aromadendrin (122850)*	• *Curcumin*
		• *Asarinin (5204)*	• *(969516)*
		• *Choline (305)*	• *Flavylium*
		• *Menthalactone (94349)*	• *(145858)*
		• *Santonin (221071)*	• *Ginkgotoxin (76581)*
		• *L-Rhamnose (25310)*	• *Globosterol (53477610)*
2	*Boswellia serrata*	• *1-Isopropyl-4-Methylenebicyclo [3.1.0]Hex-2-Ene (524198)*	• *Epicubenol (12046149)*
		• *10-Epi-Gamma-Eudesmol (6430754)*	• *Methylisoeugenol (637776)*
		• *3,5-Dimethoxytoluene (77844)*	• *Serratol (86577759)*
		• *Alpha-Campholenic-Acid (12302349)*	• *Terpinolene (11463)*
			• *Tricyclene (79035)*
			• *Undecenol (22506525)*
			• *Beta-Ocimene (18756)*

(*Continued*)

Table 2. (*Continued*)

Sl No:	Plant	Phytocompound *(PubChem ID)*	
3	*Glycyrrhiza glabra*	• *(1r,3s,4r,7r,9s,12s,13r,17s,19r,20r,22s)-9-Hydroxy-3,4,8,8,12,19,22-Heptamethyl-14-Oxo-23-Oxahexacyclo[18.2.1.03,16.04,13.07,12.017,22] Tricos-15-Ene-19-Carboxylic Acid (88302)*	• *Dihydro-5,5-Dimethyl-2(3h)-Furanone (18398)*
		• *2,3,5-Trimethylpyrazine (26808)*	• *Ethyl Phenylacetate (759)*
		• *2,3-Butanediol (262)*	• *Geraniol (637566)*
		• *2,4-Difurfurylfuran (53423642)*	• *Hydroxyacetone (8299)*
		• *2-(4-Methylphenyl)Propan-2-Ol (255195)*	• *Lavandulol (5464156)*
		• *2-Acetyl-1-Furfurylpyrrole (20560368)*	• *Ligustrazine (14296)*
		• *2-Acetyl-5-Methylfuran (14514)*	• *N-Acetylpyrrole (521947)*
		• *2-Acetylpyrrole (14079)*	• *Oct-1-En-3-Ol (18827)*
		• *2-Ethyl-6-Methylpyrazine (26332)*	• *Piperitenone (38115)*
		• *2'-Hydroxyacetophenone (68490)*	• *Pratol (5320693)*
		• *2'-Methoxyacetophenone (77698)*	• *Texasin (5281812)*
		• *2-Pentylfuran (19602)*	• *Ambrettolide (5365703)*
		• *2-Phenylbutanoate (3881907)*	• *Anabasine (2181)*
		• *3-Methyl-3-Hepten-2-One (5364798)*	• *Cuscohygrine (1201543)*
			• *4-Aminopyridine (1727)*
			• *4-Carvomenthenol (11230)*
			• *5,6,7,8-Tetrahydro-2,4-Dimethylquinoline (185667)*
			• *4-Methylcoumarin (11833)*
			• *6-Prenylnaringenin (155094)*
			• *7-Methoxyco33umarin (10748)*
4	*Scoparia dulcis*	• *2-Benzoxazolinon (6043)*	
5	*Withania somnifera*	• *Anahygrine (12306778)*	
		• *Delta-Cadinene (441005)*	
		• *Nicotine (89594)*	

Table 3. Grid box generated for ten proteins

	DIMENSIONS			*GRID CENTER*		
PROTEIN	x	y	z	x	y	z
TNF	80	86	94	−17.917	22.960	−23.170
IL-6	100	84	76	−14.705	−19.582	0.322
MMP9	126	126	126	−5.117	−0.711	−12.712
ACE	126	112	120	5.222	0.000	0.000
NF-kB105	86	84	68	−22.000	−20.376	4.558
MMP2	102	108	112	−15.608	10.200	4.171
TIMP1	106	48	66	−12.349	0.740	−1.249
TIMP2	74	100	66	−0.330	−12.900	−1.223
C3	126	126	126	−11.969	9.930	9.493
CD55	126	126	126	0.454	8.693	2.696

10.353 × 8.398 nm, resulting in a volume of 893.44 nm³. The periodic boundary conditions are applied in all three dimensions (X, Y, and Z). Then the systems were solvated within a dodecahedron box utilizing the transferable intermolecular potential with a three-point (TIP3P) water model, followed by addition of ions (neutralization using Na+ and Cl− ions). Employing the steepest descent integrator, energy minimization was performed to resolve steric conflicts between proteins and water molecules. After energy minimization, ligand restraining and temperature coupling were performed. The modified Berendsen thermostat (V-rescale) is applied in the simulation to control the temperature of both the protein-ligand complex and the solvent (water and ions) [36]. This ensures that the system's kinetic energy remains stable at the desired reference temperature of 300 K throughout the simulation. The systems were subjected to volume equilibration – NVT ensemble (constant number of particles, volume, and temperature) and followed by equilibration of pressure – NPT ensemble, by keeping the number of particles (N), the system pressure (P), and the temperature (T) constant. Both steps were carried out for 1, 00,000 steps, resulting in a cumulative time of 200 ps. A pressure of 1 atm and temperature of 300 k were sustained. A production molecular dynamics run of 50,000,000 steps was performed for 100 ns, as demonstrated in studies exploring the interaction of TNF-α with saponins from Vietnamese ginseng and the binding of NF-κB protein with sulindac acid [37, 38].

2.8. Trajectory analysis

Analysis of the resulting trajectories encompassed various aspects, including root mean square deviation (RMSD), root mean square fluctuation (RMSF), SASA, radius of gyration (*Rg*), and H-bond interactions, utilizing the GROMACS version 2020.1 package. Trajectory plot analysis was executed using Xmgrace. The stability validation of the protein and the complexes was performed by comparative analysis of RMSD and RMSF. The protein compactness was studied by plotting the *Rg*. The number of Hydrogen bonds formed between the protein and ligands for 100 ns was depicted. For visualizing the post-MD simulation complexes, tools such as DS Visualizer, Visual Molecular Dynamics, and Pymol were employed. Dynamic Cross-Correlation Matrix analysis was also carried out to understand how different atoms within a molecule move in relation to each other. This method calculates the dynamic cross-correlation between residue pairs, producing a matrix. Each element in this matrix shows the correlation coefficient, indicating the extent to which the movements of two atoms are linked.

2.9. Molecular Mechanics/Poisson-Boltzmann Surface Area (MMPBSA)

The docked complex poses considered for MD simulation were also subjected to MMPBSA, to estimate the binding-free energy. gmx_mmpbsa

tool [39] developed for GROMACS was employed for MMPBSA calculations. The binding energy was further decomposed on the per-residue basis to estimate the binding-free energy of individual residue to the MGAM-TW/WA interaction. The estimation of binding-free energy of ligand-protein complexes in a solvent can be calculated by

$$\Delta G\,bind = \Delta G\,complex - [\Delta G\,protein + \Delta G\,lig] \quad (1)$$

ΔG complex – overall free energy of the complex, ΔG protein – free energy of isolate protein, ΔG lig – free energy of isolate ligand,

Conceptually, the MMPBSA approach can be explained as

$$\Delta G\,bind = \Delta E\,gas + \Delta G\,sol = \Delta E\,vdw + \Delta E\,ele + \Delta G\,polar + \Delta G\,nonpolar \quad (2)$$

where ΔE gas (gas-free energy) = average molecular mechanic potential energy in a vacuum (van der Waals (ΔE vdw) + electrostatic (ΔE ele) interactions),

$$\Delta G\,sol = polar\ solvation\ (\Delta G\,polar)\ energy + nonpolar\ solvation\ (\Delta G\,nonpolar)\ energy \quad (3)$$

3. Result and Discussion

In silico analysis of the multiple targets and phytocompounds (Curcumin, *Ginkgo biloba*, *Boswellia serrata*, Astragalus, Ashwagandha, *Glycyrrhiza glabra*, and *Scoparia dulcis*) was performed to identify potential molecules for the treatment of LN. The methodology employed for this analysis encompassed Data mining, Network analysis, Molecular and physicochemical property calculation and Screening of Ligands, Molecular docking, Interaction Analysis, Molecular dynamic simulation, Trajectory analysis, and MMPBSA calculations.

The initial data set of receptor and ligand molecules was subjected to various analyses, and the 10 targets – TNF, IL-6, matrix metalloproteinase (MMP9 & MMP2) ACE, NF-kB105, tissue inhibitor matrix metalloproteinase 1 (TIMP1 & TIMP2), complement component 3 (C3) and complement DAF (CD55) and 65 ligands were considered for the study. Out of the listed 1526 ligands, only 65 satisfied the rule and filtering parameters. The molecular docking results were screened and ranked based on binding affinity and no of h-bond interactions. The top-ranked 10 poses from each target are compiled in Table 4.

Dock results of the phytocompounds against the targets exhibit the binding affinity ranges from −9.6 kcal/mol to −5.8 kcal/mol. Among the top-ranked 100 ligand poses from 10 dock complexes, the top 3 ligands from each target (total 30) were carried out for the next level of analysis, i.e., MD simulations to validate the interaction stability.

Phytocompounds that interact with TNF include Asarinin (ARG 107, ASN 122; −6.9 kcal/mol), 6-Prenylnaringenin (GLU 192, GLU 186; −6.6 kcal/mol), and Cianidanol (LEU 218, PHE 220, PRO 215; −6.5 kcal/mol) and those interact with IL-6 include 6-Prenylnaringenin (SER 204, GLU 87; −7.1 kcal/mol), Aromadendrin (GLU 200; −6.9 kcal/mol), and Cianidanol (MET 95, LEU 193, ARG 196, SER 204; −6.8 kcal/mol). The ligands which show better binding affinity towards MMP9 include 1r, 3s, 5r-6, 6-Dimethyl-2-methylidene-bicyclo [3.1.1] heptan-3-ol (LYS 461, ASP 422; −8.6), Asarinin (TRP 825, ASN 816, TYR 740; −8.6), and Santonin (HIS 520, HIS 360; −8.2), whereas Asarinin (ARG 125, SER 229; −9.4), Santonin (HIS 360, HIS 520; −8.6),

Table 4. Top-ranked 10 receptor ligand poses from each target

Sl No:	Protein	Name	H-bond	No. of H-bonds	Binding affinity (kcal/mol)
1	TNF	Asarinin	ARG 107, ASN 122	2	−6.9
2		6-Prenylnaringenin	GLU 192, GLU 186	2	−6.6
3		Cianidanol	LEU 218, PHE 220, PRO 215	3	−6.5
4		Pratol	GLY 224	1	−6.5
5		Globosterol	GLY 184, ALA 185, CYS 145	3	−6.4
6		Flavylium	ASN 122	1	−6.1
7		Aromadendrin	ALA 160, ARG 158, THR 165, TYR 163	4	−6
8		Santonin	GLN 178, ARG 179	2	−6
9		Texasin	PRO 182, GLY 184, ALA 185	3	−6
10		4-Methylcoumarin	VAL 226, GLN 225	2	−5.9
1	Interleukin-6	6-Prenylnaringenin	SER 204, GLU 87	2	−7.1
2		Aromadendrin	GLU 200	1	−6.9
3		Cianidanol	MET 95, LEU 193, ARG 196, SER 204	4	−6.8
4		Asarinin	ASN 172	1	−6.7
5		Curcumin	LEU 92, LYS 114	2	−6.5
6		Texasin	GLU 200, SER 204, PRO 93, PHE 201	4	−6.5
7		Flavylium	GLN 203		−6.1
8		Globosterol	SER 136, GLU 70	2	−6
9		Pratol	THR 71, SER 75, LYS 74, GLU 134, ARG 132	5	−6
10		10-epi-gamma-Eudesmol	GLU 121	1	−5.8

(*Continued*)

Table 4. (*Continued*)

Sl No:	Protein	Name	H-bond	No. of H-bonds	Binding affinity (kcal/mol)
1	MMP9	1r,3s,5r-6,6-Dimethyl-2-methylidene-bicyclo [3.1.1] heptan-3-ol	LYS 461, ASP 422	2	−8.6
2		Asarinin	TRP 825, ASN 816, TYR 740	3	−8.6
3		Santonin	HIS 520, HIS 360	2	−8.2
4		Ginkgotoxin	ASN 816	1	−8.2
5		2,3,5-Trimethylpyrazine	TRP 825, ARG 729	2	−8.2
6		Anabasine	ARG 729, TRP 825	2	−8.2
7		2-Benzoxazolinone	ASN 816	1	−8.1
8		Aromadendrin	TYR 530, HIS 520, THR 525	3	−8
9		Choline	LEU 168, ASP 169	2	−7.7
10		Rhamnose	GLU 418, HIS 360, HIS 520, GLU 391, HIS 394	4	−7.2
1	ACE	Asarinin	ARG 125, SER 229	2	−9.4
2		Santonin	HIS 360, HIS 520	2	−8.6
3		Aromadendrin	GLU 418, HIS 520, TYR 530, THR 525, ASP 72, TYR 398	6	−8.6
4		Globosterol	HIS 1118, HIS 992, GLU 989	3	−8.4
5		6-Prenylnaringenin	TYR 530, HIS 360, HIS 520, GLU 391, HIS 390, HIS 394	6	−8.3
6		Ambrettolide	TYR 1128	1	−8.2
7		Cianidanol	LYS 973, ASN 675, GLU 7448	3	−8.2
8		Pratol	GLU 767, LYS 1116	2	−8.1
9		Texasin	ARG 409, ASP 365	2	−8.1
10		Curcumin	ASN 523, SER 362, ASP 365, TYR 398	4	−7.9
1	NF-kappa-B p105	6-Prenylnaringenin	PRO 93, SER 197	2	−7.3
2		Texasin	PHE 201, GLU 200, SER 204, PRO 93	4	−7
3		Asarinin	ASN 172	1	−6.8
4		Cianidanol	LEU 193, ARG 196, MET 95, SER 204	4	−6.8
5		Curcumin	LEU 92, LYS 114	2	−6.5
6		Aromadendrin	ARG 207, SER 197	2	−6.3
7		Flavylium	GLN 203	1	−6.2
8		Globosterol	PRO 169	1	−6.2
9		Santonin	SER 104, GLN 103	2	−6.1
10		Pratol	THR 71, SER 75, ARG 132, LYS 74, GLU 134	5	−6
1	MMP2	Globosterol	ALA 959, GLU 989	2	−9.6
2		Asarinin	TYR 965, ALA 961, HIS 958, HIS 988	4	−9.3
3		Santonin	HIS 360, HIS 520	2	−8.6
4		6-Prenylnaringenin	GLN 886, ASP 1020	2	−8.5
5		Aromadendrin	TYR 1128, HIS 1118	2	−8.4
6		Cianidanol	GLU 1016, TYR 1128, GLU 748, ASN 675, ALA 961	5	−8.2
7		Curcumin	LYS 518, VAL 357	2	−8.2
8		Serratol	THR 387	1	−8.2
9		Pratol	HIS 958, TYR 1128, HIS 1118, ASN 675	4	−8.1
10		Ambrettolide	GLN 288, SER 289	2	−7.8
1	TIMP1	Asarinin	THR 120, GLN 113	2	−8.1
2		Aromadendrin	ALA 34, SER 38	2	−7.8
3		Pratol	SER 38	1	−7.7
4		Globosterol	HIS 118	1	−7.6

(Continued)

Table 4. (*Continued*)

Sl No:	Protein	Name	H-bond	No. of H-bonds	Binding affinity (kcal/mol)
5		6-Prenylnaringenin	SER 130, GLN 135, SER 123	3	−7.5
6		Curcumin	VAL 125, SER 130, ARG 185	3	−7.4
7		Cianidanol	PHE 124, ALA 109, SER 38	3	−7.3
8		Texasin	SER 38, ALA 34, ALA 109, PHE 124	4	−7.1
9		Santonin	HIS 97, SER 99, ARG 98	3	−6.4
10		Flavylium	ASN 53	1	−6.4
1	TIMP2	Aromadendrin	THR 135, LEU 126	2	−7.5
2		6-Prenylnaringenin	ASP 128, LEU 126, ILE 183	3	−7.2
3		Asarinin	ARG 68	1	−7.1
4		Globosterol	LEU 126, ASP 128	2	−6.9
5		Serratol	VAL 32	1	−6.8
6		Texasin	VAL 32, ILE 130	2	−6.6
7		Cianidanol	VAL 32, LEU 126	2	−6.6
8		Curcumin	LEU 126	1	−6.5
9		Pratol	ASP 176, GLU 180, THR 179	3	−6.4
10		Santonin	VAL 32	1	−6.4
1	C3	Asarinin	ARG 1532, HIS 1630, GLN 1521	3	−9
2		Globosterol	ARG 1532, GLN 1645, ASP 1525	3	−8.4
3		6-Prenylnaringenin	LYS 1431	1	−8.2
4		Cianidanol	LYS 927, THR 800, ASP 599	3	−7.9
5		Pratol	ARG 834, ASN 1442	2	−7.8
6		Aromadendrin	ASP 599, SER 798, LYS 927, ASP 832	4	−7.6
7		Santonin	ARG 834, TYR 852	2	−7.6
8		Ambrettolide	ILE 799	1	−7.5
9		Serratol	TYR 852	1	−7.5
10		Curcumin	GLN 216, SER 219, LYS 615, ASN 609	4	−7.4
1	CD55	Globosterol	HIS 1118, HIS 992, GLU 989	3	−9.6
2		Asarinin	ARG 125, SER 229	2	−9.1
3		Pratol	LYS 1116, GLU 767	2	−8.7
4		Aromadendrin	GLU 418, HIS 520, TYR 530, THR 525, ASP 72, TYR 398	6	−8.6
5		Santonin	HIS 520, HIS 360	2	−8.6
6		6-Prenylnaringenin	TYR 53.0, HIS 360, HIS 520, GLU 391, HIS 390, HIS 394	6	−8.4
7		Texasin	ARG 409, ASP 365	2	−7.7
8		Serratol	GLN 288	1	−7.7
9		Cianidanol	LYS 973, TYR 667	2	−7.5
10		Ambrettolide	HIS 520, TYR 530	2	−7.4

Aromadendrin (GLU 418, HIS 520, TYR 530, THR 525, ASP 72, TYR 398; −8.6) shows better interaction with ACE. Those ligands which show highest binding affinity with NF-kappa-B p105 were 6-Prenylnaringenin (PRO 93, SER 197; −7.3), Texasin (PHE 201, GLU 200, SER 204, PRO 93; −7), and Asarinin (ASN 172; −6.8). Likewise, Globosterol (ALA 959, GLU 989; −9.6), Asarinin (TYR 965, ALA 961, HIS 958, HIS 988: −9.3), Santonin (HIS 360, HIS 520; −8.6) shows good interaction with the protein MMP2, Asarinin (THR 120, GLN 113; −8.1), Aromadendrin (ALA 34, SER 38; −7.8), Pratol (SER 38: −7.7) with TIMP1, Asarinin (ARG 1532, HIS 1630, GLN 1521; −9), Globosterol (ARG 1532, GLN 1645, ASP 1525; −8.4), 6-Prenylnaringenin (LYS 1431; −8.2) interact with C3 and Globosterol (HIS 1118, HIS 992, GLU 989; −9.6), Asarinin (ARG 125, SER 229: −9.1) & Pratol (LYS 1116, GLU 767; −8.7) exhibit better interaction with CD55.

The interaction stability of these 30 complexes was analyzed. The result contains both stable and unstable interactions. Few ligands maintain interactions with the same amino acid residues as observed in the molecular docking result. In contrast, others exhibit distinct interactions, primarily attributed to energy fluctuations and changes in conformational geometry. After molecular dynamics simulation, the trajectories were analyzed to understand the spatial fluctuations of protein. Among the subjected 30 ligand molecules, only 2 receptor-ligand complexes – NF-kappa105_6-prenylnaringenin and TNF_6-Prenylnaringenin

Table 5. Receptor ligand interaction after MD simulation and MMPBSA result

Sl No:	Protein	Name	H-Bond	Affinity (kcal/mol)	MD	MMPBSA (kcal/mol)
1	NF-kappa-B p105	6-Prenylnaringenin	PRO 93, SER 197	−7.3	GLU 87, ASN 88, SER 197, PRO 93	−15.38
2	TNF	6-Prenylnaringenin	GLU 192, GLU 186	−6.6	TYR 191, GLU 192, GLU 186, LYS 188	−23.26

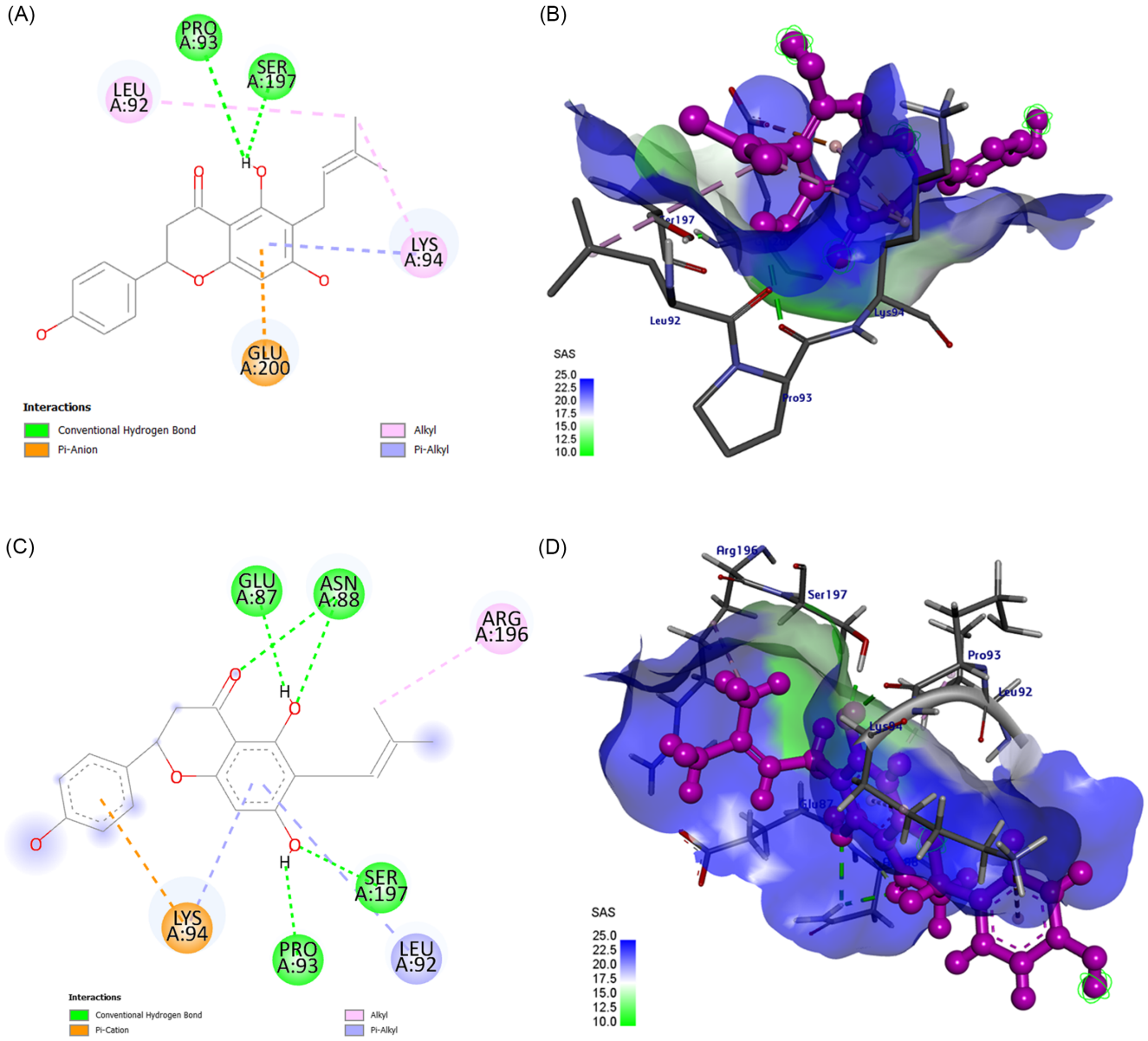

Figure 3. (A) 2D interaction diagram of NF-kappa105_6-prenylnaringenin dock complex. (B) 3D interaction diagram of NF-kappa105_6-prenylnaringenin dock complex. (C) 2D interaction diagram of NF-kappa105_6-prenylnaringenin MD complex. (D) 3D interaction diagram of NF-kappa105_6-prenylnaringenin MD complex

show stable interactions. The MMPBSA of the complexes was calculated (Table 5).

The compound's favorable binding energies and interaction stability may indicate their potency. The least binding affinity constitutes the strongest binding.

In the NF-kappa105_6-prenylnaringenin complex, the dock result has 2 h-bonds at PRO 93, SER 197 residues with a binding affinity of −7.3 kcal/mol, and after molecular dynamic simulation, the complex exhibit 4 h-bonds at GLU 87, ASN 88, SER 197, and PRO 93, in which the SER 197 residue remains

stable (Figure 3). Also, the complex shows −15.38 kcal/mol binding-free energy. The RMSD values vary from a minimum of 0.2794797 nm at 0.1 ns to a maximum of 2.3947103 nm at 94.2000046 ns. The RMSF plot of the NF-kappa105_6-prenylnaringenin complex shows that the entire protein shows fluctuation between 0.2453 nm and 2.9046 nm. Among these, MET 1 (2.9046 nm) has the highest fluctuation. In between 0 ns and 50 ns, significant fluctuations (black line) were observed in the region of residues from 50 to 150. These fluctuations point out that the residues are undergoing substantial conformational adjustments as they adapt to the simulation environment, attaining equilibrium. During 50 ns – 100 ns, the fluctuations were significantly reduced, particularly in the same residue range (50–150) which exhibited high fluctuations in the initial phase. This indicates attaining stability (protein residues exhibiting less dynamic movement and more stable interactions) compared to the initial phase of the system. The RoG plot of NF-kappa105_6-prenylnaringenin inferred that the *Rg* deviation ranges from 2.69639 nm (63.2 ns) to 3.52186 nm (4.4 ns) with an average of 3.15635013 nm. A maximum of 5 H-bonds was observed during the 100 ns MD simulation (Figure 4).

For TNF_6-Prenylnaringenin complex, the dock result has 2 h-bonds at GLU 192, GLU 186 residues with a binding affinity of −6.6 kcal/mol, and after molecular dynamic simulation, the complex exhibits 4 h-bonds at TYR 191, GLU 192, GLU 186, LYS 188 residues in which the GLU 192, GLU 186 residues remain stable (Figure 5). The complex shows −23.26 kcal/mol binding-free energy. The RMSD values of the plot vary from a minimum of 0.3118211 nm at 0.1 ns to a maximum of 2.7302127 nm at 44.80 ns. The RMSF plot of the TNF_6-Prenylnaringenin complex shows that the entire protein shows fluctuation between 0.2507 nm and 1.7259 nm. Among these, MET 1 (1.7259 nm) has the highest fluctuation. Within the 0 to 50 ns timeframe, notable fluctuations (black line) were evident in residues 50 to 150, indicating significant conformational changes as the residues adjusted to the simulation environment, seeking equilibrium. As the simulation progressed to the 50 to 100 ns range, these fluctuations significantly decreased, particularly within the same residue range (50–150) that exhibited high fluctuations initially. This reduction suggests that the protein residues have achieved greater stability, demonstrating less dynamic movement and more stable interactions compared to the early

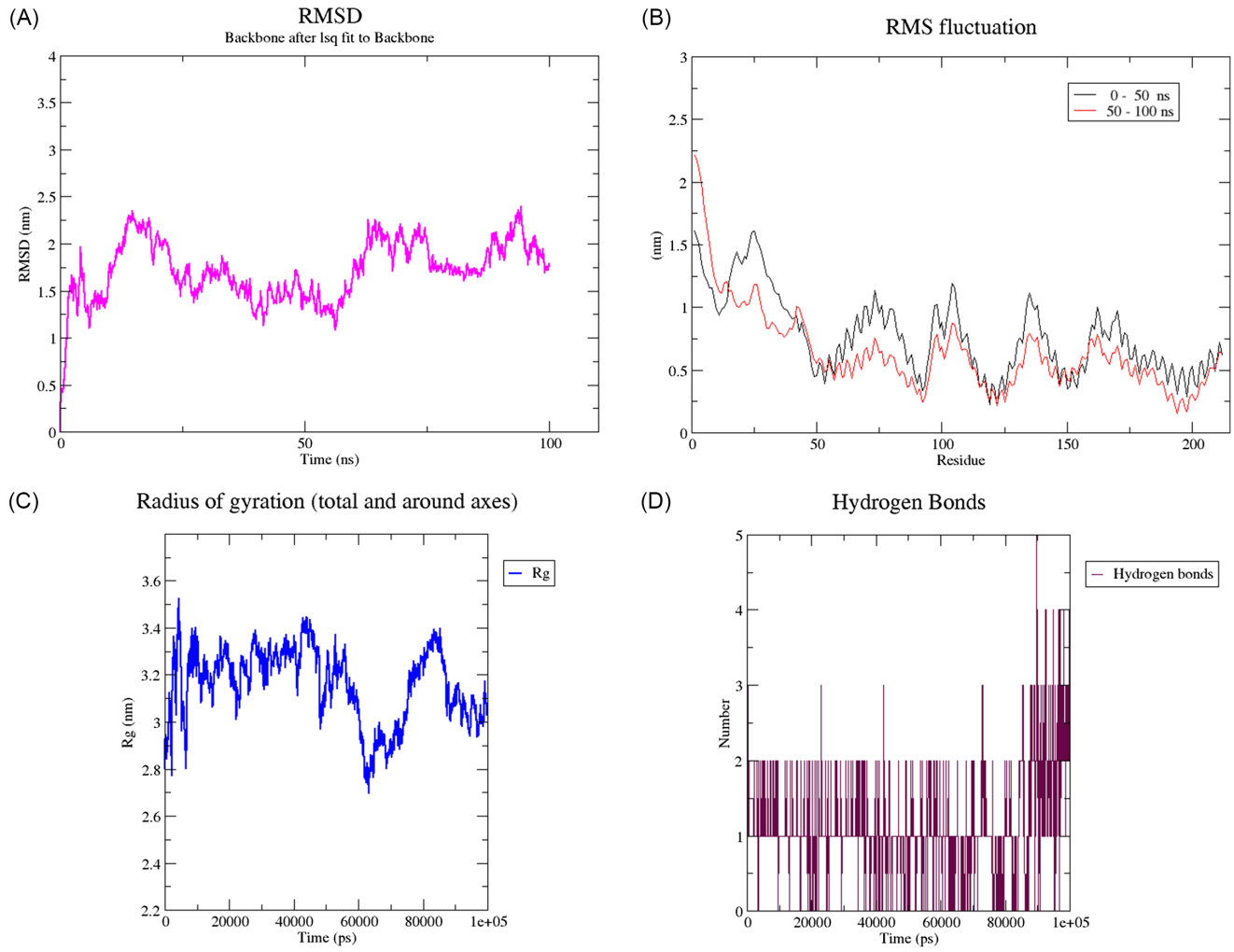

Figure 4. (A) RMSD plot of NF-kappa105_6-prenylnaringenin complex. (B) RMSF plot of NF-kappa105_6-prenylnaringenin complex. (C) RoG plot of NF-kappa105_6-prenylnaringenin complex. (D) H-bond distribution plot of NF-kappa105_6-prenylnaringenin complex

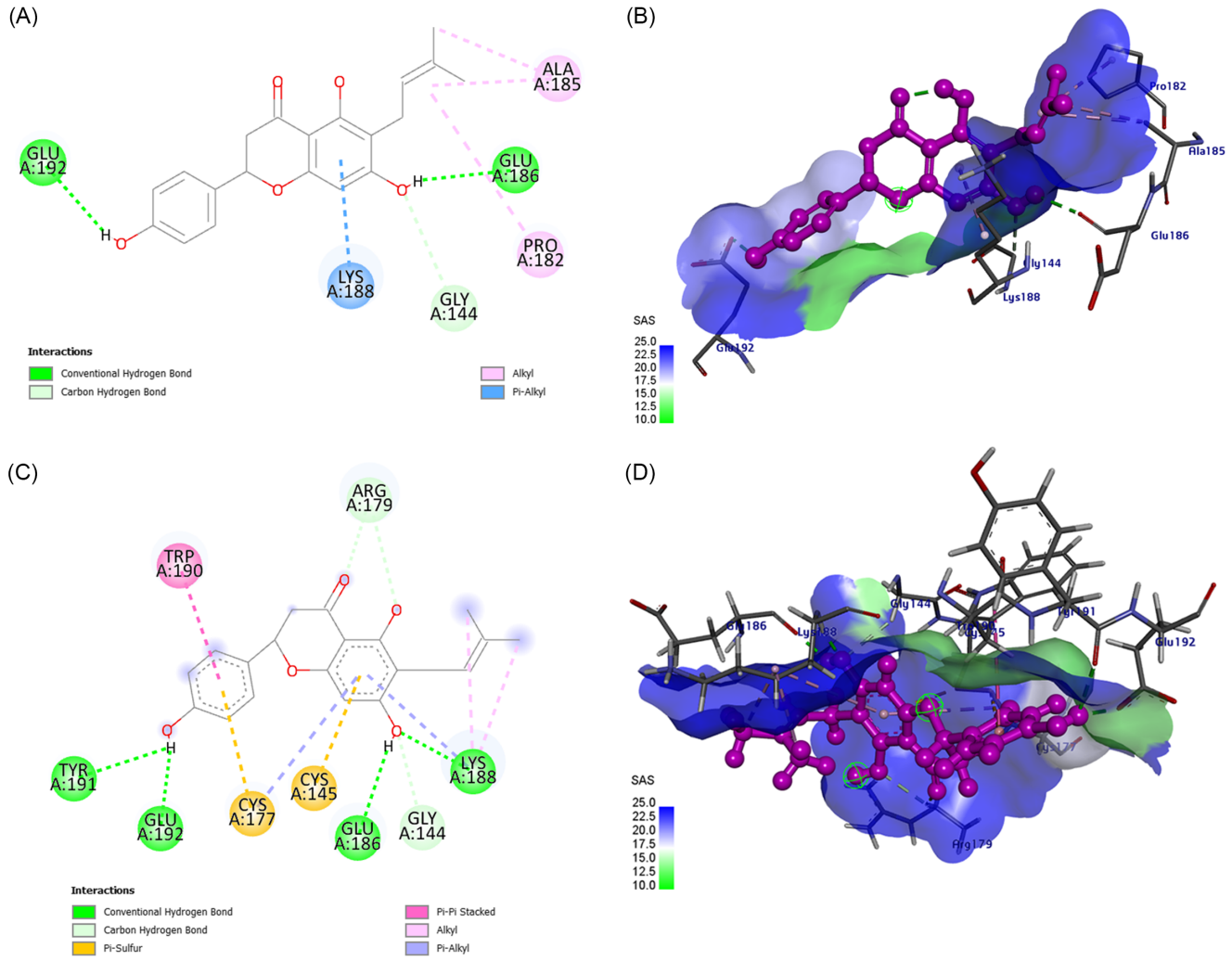

Figure 5. (A) 2D interaction diagram of TNF_6-Prenylnaringenin dock complex. (B) 3D interaction diagram of TNF_6-Prenylnaringenin dock complex. (C) 2D interaction diagram of TNF_6-Prenylnaringenin MD complex. (D) 3D interaction diagram of TNF_6-Prenylnaringenin MD complex

phase of the system. The RoG plot of TNF_6-Prenylnaringenin inferred that the *Rg* deviation ranges from 2.16984 nm (82.90 ns) to 3.96803 nm (3.9 ns) with an average of 2.565139251 nm. A maximum of 6 H-bonds was observed during the 100 ns MD simulation (Figure 6). The dynamic cross-correlation between residue pairs of the complex of TNF_6-Prenylnaringenin and TNF_6-Prenylnaringenin are depicted in Figures 7 and 8, respectively. The insights derived from Figures 7 and 8 are summarized in Table 6.

The study underscores the potential of 6-Prenylnaringenin as a promising drug candidate for the treatment of LN. The phytocompound shows stable interactions with the target protein NF-kappa B 105 (NF-κB p105) and TNF, which are significant in the inflammatory pathways associated with LN. These interactions were maintained throughout the simulation, indicating strong binding affinities and interaction stability. The binding affinity of 6-Prenylnaringenin to NF-κB p105 and TNF suggests that it may effectively inhibit these proteins' activity, thereby reducing inflammation and immune response dysregulation. Such modulation of inflammatory pathways is critical in managing LN, where excessive immune responses cause significant kidney damage. Additionally, the robust hydrogen bonding and interaction stability observed post-molecular dynamic simulations further emphasize the therapeutic potential of 6-Prenylnaringenin. The RMSF analysis also indicates that the protein-ligand complex maintains stability over time, which is vital for its efficacy as a therapeutic agent. Overall, this in silico study demonstrates the potential of 6-Prenylnaringenin as a clinical candidate for LN treatment. Its ability to interact with NF-κB p105 and TNF and modulate key inflammatory pathways underscores its promise in developing new therapeutic strategies for this challenging autoimmune condition. Further experimental validation and clinical studies would be necessary to confirm these findings and translate them into practical medical applications.

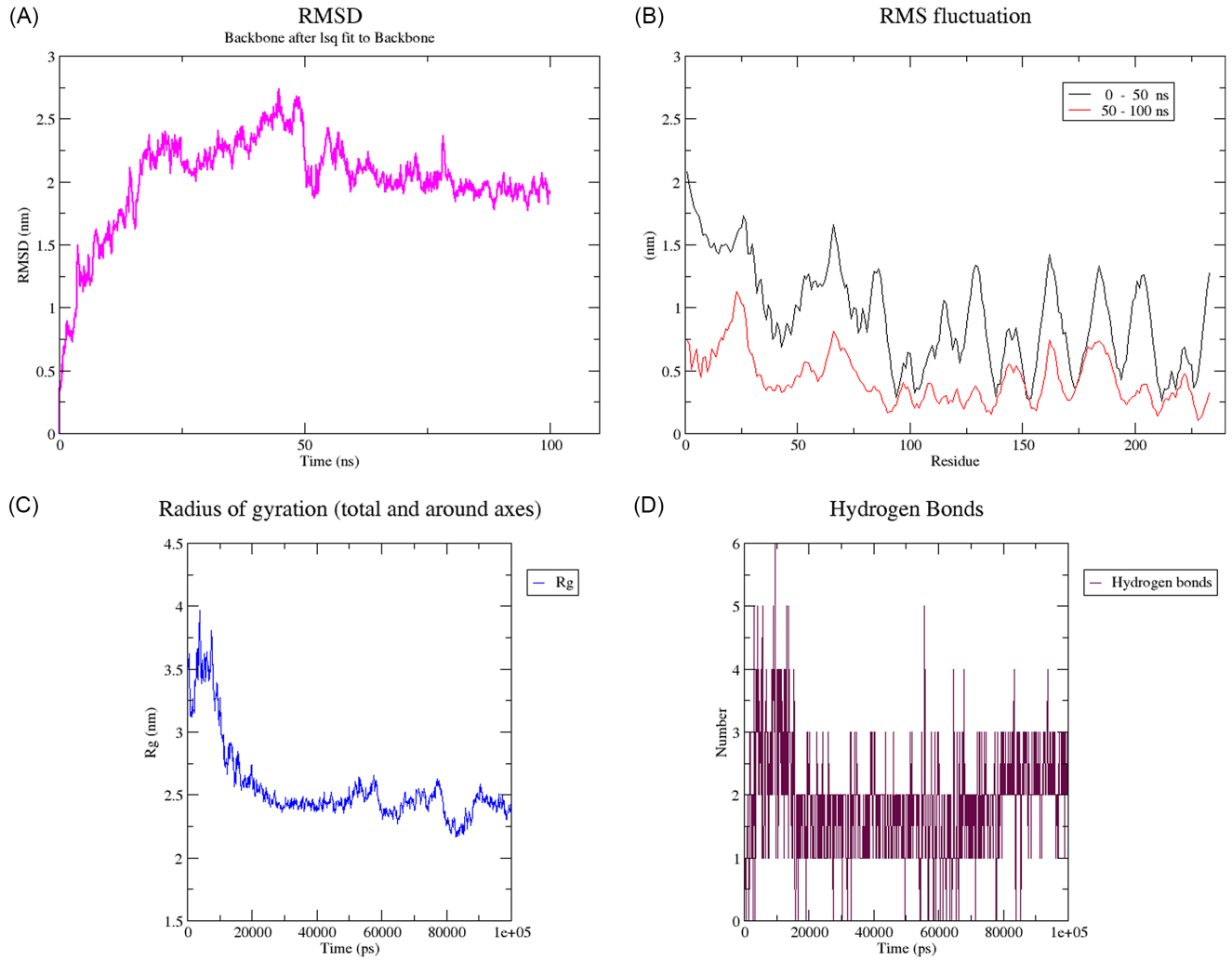

Figure 6. (A) RMSD plot of TNF_6-Prenylnaringenin complex. (B) RMSF plot of TNF_6-Prenylnaringenin complex. (C) RoG plot of TNF_6-Prenylnaringenin complex. (D) H-bond distribution plot of TNF_6-Prenylnaringenin complex

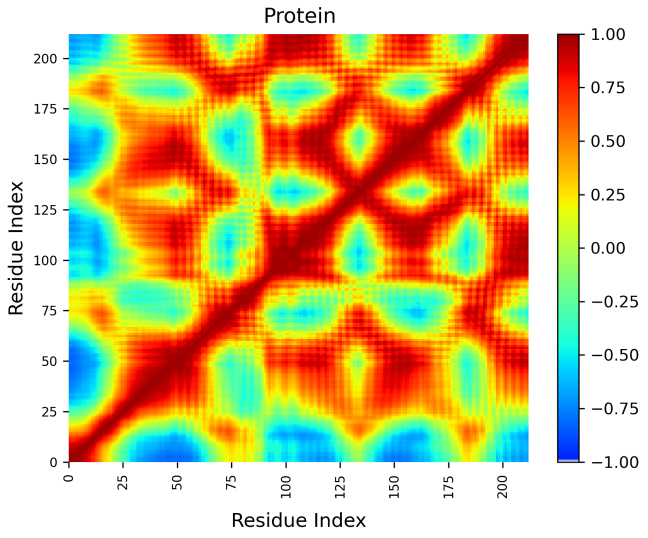

Figure 7. Heat map of NF-kappa105_6-prenylnaringenin complex

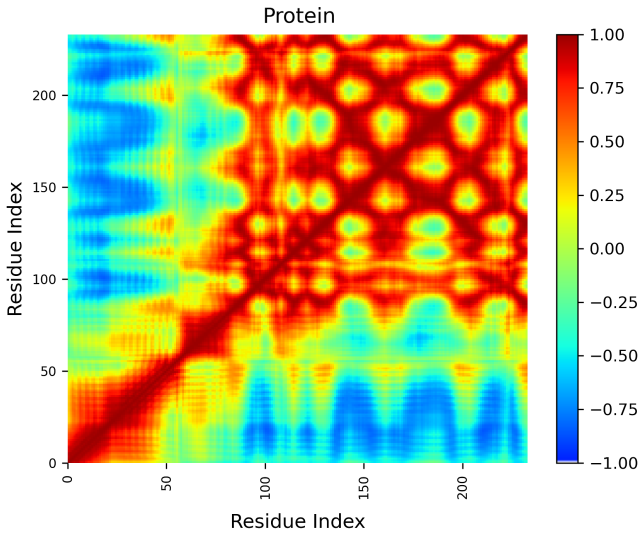

Figure 8. Heat map of TNF_6-Prenylnaringenin complex

Table 6. Inference of heat map NF-kappa105 (Figure 7) and TNF (Figure 8)

	NF-kappa105		TNF		
Correlation type	Residue index (i)	Residue index (j)	Residue index (i)	Residue index (j)	Description
Diagonal Line	i = j	i = j	i = j	i = j	Bright red diagonal line representing self-correlation, where each residue is perfectly correlated with itself (correlation = 1).
Strongly Correlated	0–50	0–50	0–75	0–75	Large red region in the top-left corner, indicating these residues move together, possibly part of an α-helix or β-sheet.
Strongly Correlated	150–200	150–200	100–200	100–200	Large red region in the lower right corner, suggesting these residues move together as a unified domain.
Moderately Correlated	50–100	100–150	75–150	150–225	Yellow to orange regions, indicating moderate positive correlation and coordinated movement, but with more flexibility.
Anti-Correlated	50–100	0–50	0–75	150–225	Significant blue region, suggesting these segments move in opposite directions, possibly acting as a hinge.
Anti-Correlated	100–150	150–200	75–150	0–75	Blue patch supporting opposing movements between different domains or subdomains.
Uncorrelated	0–50	150–200	0–75	150–225	Green areas showing little to no correlation, indicating independent movements of spatially distant or dynamically independent residues.
Uncorrelated	50–100	150–200	75–150	150–225	Green regions indicating structurally or functionally independent movement.

4. Conclusion

The study employs various computational techniques to screen and evaluate the effectiveness of phytocompounds derived from traditional medicinal plants as potential ligands targeting key protein molecules associated with the pathway of LN disorder. A total of 65 ligands and 10 targets – TNF, IL-6, matrix metalloproteinase (MMP9 & MMP2) ACE, NF-kB 105, tissue inhibitor matrix metalloproteinase 1 (TIMP1 & TIMP2), complement component 3 (C3), and complement DAF (CD55) were considered for the in silico analysis. The study incorporated various bioinformatics approaches such as data mining, molecular property calculation, molecular docking, molecular dynamic simulation, and MMPBSA. The molecular interaction analysis, along with molecular dynamics simulation, indicates that two ligand molecules – 6-Prenylnaringenin and Cianidanol – show stable and favorable interactions with the targets. Among these, 6-Prenylnaringenin exhibits binding affinity towards multiple targets, NF-kappa105 (−7.3 kcal/mol), and TNF (−6.6 kcal/mol). Further in-vitro analysis is needed for the validation of the potency of the identified lead molecule.

To confirm the potential of these phytocompounds against LN beyond the constraints involved in the computational study, further in vitro analysis and clinical research are needed. In vitro study will provide better understanding about the safety and effectiveness of the compounds in the treatment of LN. The study provides more insights into the role of selected targets in LN, and the scope of isolation of these lead molecules in treatment of LN These studies will also help in confirming the real-world therapeutic potential of 6-Prenylnaringenin, focusing on its mechanism of action, dosage, and impact in clinical settings. They will bridge the gap between computational insights and practical applications, offering a more forward-looking perspective on developing effective treatments for LN. Furthermore, exploring the potential of the lead candidate in animal models could pave the way for the development of effective herbal-based treatments for this complex disorder.

Acknowledgment

This research was supported by Accubits Invent Pvt. Ltd. and supervised by Dr. Nidhin Sreekumar, Chief Research Scientist. We thank all our colleagues who provided insight and expertise that greatly assisted the research.

Conflicts of Interest

The authors declare that they have no conflicts of interest to this work.

Data Availability Statement

Data sharing is not applicable to this article as no new data were created or analyzed in this study.

Author Contribution Statement

Shahanas Naisam: Conceptualization, Methodology, Writing – original draft, Visualization. **Aswin Mohan:** Validation, Formal analysis, Investigation, Writing – original draft. **Gayathri Sreedevi Sivakumar:** Formal analysis, Writing – original draft, Writing – review & editing. **Sagarkrishna Gopalakrishnan:** Investigation, Data curation, Writing – original draft. **Nidhin Sreekumar:** Resources, Supervision, Project administration.

References

[1] Fava, A., & Petri, M. (2019). Systemic lupus erythematosus: Diagnosis and clinical management. *Journal of Autoimmunity*, *96*, 1–13. https://doi.org/10.1016/j.jaut.2018.11.001

[2] Kiremitci, S., & Ensari, A. (2014). Classifying lupus nephritis: An ongoing story. *The Scientific World Journal*, *2014*(1), 580620. https://doi.org/10.1155/2014/580620

[3] Stokes, M. B., & D'Agati, V. D. (2019). Classification of lupus nephritis; time for a change? *Advances in Chronic Kidney Disease*, *26*(5), 323–329. https://doi.org/10.1053/j.ackd.2019.06.002

[4] Ameer, M. A., Chaudhry, H., Mushtaq, J., Khan, O. S., Babar, M., Hashim, T., ..., & Hashim, S. (2022). An overview of systemic lupus erythematosus (SLE) pathogenesis, classification, and management. *Cureus*, *14*(10), e30330. https://doi.org/10.7759/cureus.30330

[5] Renaudineau, Y., Brooks, W., & Belliere, J. (2023). Lupus nephritis risk factors and biomarkers: An update. *International Journal of Molecular Sciences*, *24*(19), 14526. https://doi.org/10.3390/ijms241914526

[6] Hasan, B., Fike, A., & Hasni, S. (2022). Health disparities in systemic lupus erythematosus—A narrative review. *Clinical Rheumatology*, *41*(11), 3299–3311. https://doi.org/10.1007/s10067-022-06268-y

[7] Kuusniemi, A. M., Lapatto, R., Holmberg, C., Karikoski, R., Rapola, J., & Jalanko, H. (2005). Kidneys with heavy proteinuria show fibrosis, inflammation, and oxidative stress, but no tubular phenotypic change. *Kidney International*, *68*(1), 121–132. https://doi.org/10.1111/j.1523-1755.2005.00386.x

[8] Yuste, C., Gutierrez, E., Sevillano, A. M., Rubio-Navarro, A., Amaro-Villalobos, J. M., Ortiz, A., ..., & Moreno, J. A. (2015). Pathogenesis of glomerular haematuria. *World Journal of Nephrology*, *4*(2), 185–195. https://doi.org/10.5527/wjn.v4.i2.185

[9] Dema, B., & Charles, N. (2016). Autoantibodies in SLE: Specificities, isotypes and receptors. *Antibodies*, *5*(1), 2. https://doi.org/10.3390/antib5010002

[10] Rojas-Rivera, J. E., García-Carro, C., Ávila, A. I., Espino, M., Espinosa, M., Fernández-Juárez, G., ..., & Praga, M. (2023). Diagnosis and treatment of lupus nephritis: A summary of the consensus document of the Spanish Group for the Study of Glomerular Diseases (GLOSEN). *Clinical Kidney Journal*, *16*(9), 1384–1402. https://doi.org/10.1093/ckj/sfad055

[11] Friesner, R. A., Murphy, R. B., Repasky, M. P., Frye, L. L., Greenwood, J. R., Halgren, T. A., ..., & Mainz, D. T. (2006). Extra precision glide: Docking and scoring incorporating a model of hydrophobic enclosure for protein−ligand complexes. *Journal of Medicinal Chemistry*, *49*(21), 6177–6196. https://doi.org/10.1021/jm051256o

[12] Nikolov, A., & Popovski, N. (2021). Role of gelatinases MMP-2 and MMP-9 in healthy and complicated pregnancy and their future potential as preeclampsia biomarkers. *Diagnostics*, *11*(3), 480. https://doi.org/10.3390/diagnostics11030480

[13] Simões e Silva, A. C., Lanza, K., Palmeira, V. A., Costa, L. B., & Flynn, J. T. (2021). 2020 update on the renin–angiotensin–aldosterone system in pediatric kidney disease and its interactions with coronavirus. *Pediatric Nephrology*, *36*(6), 1407–1426. https://doi.org/10.1007/s00467-020-04759-1

[14] Liu, T., Zhang, L., Joo, D., & Sun, S. C. (2017). NF-κB signaling in inflammation. *Signal Transduction and Targeted Therapy*, *2*(1), 17023. https://doi.org/10.1038/sigtrans.2017.23

[15] Cabral-Pacheco, G. A., Garza-Veloz, I., Castruita-de la Rosa, C., Ramirez-Acuña, J. M., Perez-Romero, B. A., Guerrero-Rodriguez, J. F., ..., & Martinez-Fierro, M. L. (2020). The roles of matrix metalloproteinases and their inhibitors in human diseases. *International Journal of Molecular Sciences*, *21*(24), 9739. https://doi.org/10.3390/ijms21249739

[16] Zarantonello, A., Revel, M., Grunenwald, A., & Roumenina, L. T. (2023). C3-dependent effector functions of complement. *Immunological Reviews*, *313*(1), 120–138. https://doi.org/10.1111/imr.13147

[17] Liu, J., Miwa, T., Hilliard, B., Chen, Y., Lambris, J. D., Wells, A. D., & Song, W. C. (2005). The complement inhibitory protein DAF (CD55) suppresses T cell immunity in vivo. *The Journal of Experimental Medicine*, *201*(4), 567–577. https://doi.org/10.1084/jem.20040863

[18] Xia, S., Sun, Q., Zou, Z., Liu, Y., Fang, X., Sun, B., ..., & Liu, Q. (2020). Ginkgo biloba extract attenuates the disruption of pro-and anti-inflammatory T-cell balance in peripheral blood of arsenicosis patients. *International Journal of Biological Sciences*, *16*(3), 483–494. https://doi.org/10.7150/ijbs.39351

[19] Gandhi, G. R., & Sasikumar, P. (2012). Antidiabetic effect of *Merremia emarginata* Burm. F. in streptozotocin induced diabetic rats. *Asian Pacific Journal of Tropical Biomedicine*, *2*(4), 281–286. https://doi.org/10.1016/S2221-1691(12)60023-9

[20] Chen, H. Q., Zhang, N., Li, C. X., & Zhang, H. X. (2022). Effects of astragalus membranaceus on systemic lupus erythematosus in a mouse model of pregnancy. *Immunity, Inflammation and Disease*, *10*(6), e624. https://doi.org/10.1002/iid3.624

[21] Minhas, U., Minz, R., Das, P., & Bhatnagar, A. (2012). Therapeutic effect of *Withania somnifera* on pristane-induced model of SLE. *Inflammopharmacology*, *20*(4), 195–205. https://doi.org/10.1007/s10787-011-0102-8

[22] Vahedi-Mazdabadi, Y., & Saeedi, M. (2021). Treatment of lupus nephritis from Iranian traditional medicine and modern medicine points of view: A comparative study. *Evidence-Based Complementary and Alternative Medicine*, *2021*(1), 6645319. https://doi.org/10.1155/2021/6645319

[23] Mishra, M. R., Mishra, A., Pradhan, D. K., Panda, A. K., Behera, R. K., & Jha, S. (2013). Antidiabetic and antioxidant activity of *Scoparia dulcis* Linn. *Indian Journal of Pharmaceutical Sciences*, *75*(5), 610–614.

[24] Zhang, L., Mao, W., Guo, X., Wu, Y., Li, C., Lu, Z., ..., & Liu, X. (2013). *Ginkgo biloba* extract for patients with early diabetic nephropathy: A systematic review. *Evidence-Based Complementary and Alternative Medicine*, *2013*(1), 689142. https://doi.org/10.1155/2013/689142

[25] Shelmadine, B. D., Bowden, R. G., Moreillon, J. J., Cooke, M. B., Yang, P., Deike, E., ..., & Wilson, R. L. (2017). A pilot study to examine the effects of an anti-inflammatory supplement on eicosanoid derivatives in patients with chronic kidney disease. *The Journal of Alternative and Complementary Medicine*, *23*(8), 632–638. https://doi.org/10.1089/acm.2016.0007

[26] Sriperumbuduri, S., Umar, M. S., Lajoie-Starkell, G., Fairhead, T. R., & Hiremath, S. (2020). Ashwagandha and kidney transplant rejection. *Kidney International Reports*, *5*(12), 2375–2378. https://doi.org/10.1016/j.ekir.2020.09.024

[27] Nassan, M. A., Soliman, M. M., Aldhahrani, A., Althobaiti, F., & Alkhedaide, A. Q. (2021). Ameliorative impacts of *Glycyrrhiza glabra* root extract against nephrotoxicity induced by gentamicin in mice. *Food Science & Nutrition*, *9*(7), 3405–3413. https://doi.org/10.1002/fsn3.2183

[28] Jumper, J., Evans, R., Pritzel, A., Green, T., Figurnov, M., Ronneberger, O., ..., & Hassabis, D. (2021). Highly accurate protein structure prediction with AlphaFold. *Nature*, *596*(7873), 583–589. https://doi.org/10.1038/s41586-021-03819-2

[29] Daina, A., Michielin, O., & Zoete, V. (2017). SwissADME: A free web tool to evaluate pharmacokinetics, drug-likeness and medicinal chemistry friendliness of small molecules. *Scientific Reports*, *7*(1), 42717. https://doi.org/10.1038/srep42717

[30] Pires, D. E. V., Blundell, T. L., & Ascher, D. B. (2015). pkCSM: Predicting small-molecule pharmacokinetic and toxicity properties using graph-based signatures. *Journal of*

Medicinal Chemistry, *58*(9), 4066–4072. https://doi.org/10.1021/acs.jmedchem.5b00104

[31] Kim, S., Chen, J., Cheng, T., Gindulyte, A., He, J., He, S., . . . , & Bolton, E. E. (2019). PubChem 2019 update: Improved access to chemical data. *Nucleic Acids Research*, *47*(D1), D1102–D1109. https://doi.org/10.1093/nar/gky1033

[32] O'Boyle, N. M., Banck, M., James, C. A., Morley, C., Vandermeersch, T., & Hutchison, G. R. (2011). Open Babel: An open chemical toolbox. *Journal of Cheminformatics*, *3*(1), 33. https://doi.org/10.1186/1758-2946-3-33

[33] Eberhardt, J., Santos-Martins, D., Tillack, A. F., & Forli, S. (2021). AutoDock Vina 1.2.0: New docking methods, expanded force field, and python bindings. *Journal of Chemical Information and Modeling*, *61*(8), 3891–3898. https://doi.org/10.1021/acs.jcim.1c00203

[34] Abraham, M. J., Murtola, T., Schulz, R., Páll, S., Smith, J. C., Hess, B., & Lindahl, E. (2015). GROMACS: High performance molecular simulations through multi-level parallelism from laptops to supercomputers. *SoftwareX*, *1–2*, 19–25. https://doi.org/10.1016/j.softx.2015.06.001

[35] Páll, S., Abraham, M. J., Kutzner, C., Hess, B., & Lindahl, E. (2015). Tackling exascale software challenges in molecular dynamics simulations with GROMACS. In *Solving Software Challenges for Exascale: International Conference on Exascale Applications and Software*, 3–27. https://doi.org/10.1007/978-3-319-15976-8_1

[36] Deepasree, K., & Subhashree, V. (2023). Molecular docking and dynamic simulation studies of terpenoid compounds against phosphatidylinositol-specific phospholipase C from *Listeria monocytogenes*. *Informatics in Medicine Unlocked*, *39*, 101252. https://doi.org/10.1016/j.imu.2023.101252

[37] Kim, O. T. P., Le, M. D., Trinh, H. X., & Nong, H. V. (2016). *In silico* studies for the interaction of tumor necrosis factor-alpha (TNF-α) with different saponins from Vietnamese ginseng (*Panax vietnamesis*). *Biophysics and Physicobiology*, *13*, 173–180. https://doi.org/10.2142/biophysico.13.0_173

[38] Ahmad, S., Bhanu, P., Kumar, J., Pathak, R. K., Mallick, D., Uttarkar, A., . . . , & Mishra, V. (2022). Molecular dynamics simulation and docking analysis of NF-κB protein binding with sulindac acid. *Bioinformation*, *18*(3), 170–179. https://doi.org/10.6026/97320630018170

[39] Valdés-Tresanco, M. S., Valdés-Tresanco, M. E., Valiente, P. A., & Moreno, E. (2021). gmx_MMPBSA: A new tool to perform end-state free energy calculations with GROMACS. *Journal of Chemical Theory and Computation*, *17*(10), 6281–6291. https://doi.org/10.1021/acs.jctc.1c00645

How to Cite: Naisam, S., Mohan, A., Sivakumar, G. S., Gopalakrishnan, S., & Sreekumar, N. (2025). Discovering Potential Therapeutic Agents for Lupus Nephritis: Insights from in Silico Research. *Medinformatics*, *2*(3), 226–240. https://doi.org/10.47852/bonviewMEDIN52024089